Noise Robustness of Irregular LBP Pyramids

Christoph Körner, Ines Janusch, Walter G. Kropatsch

Pattern Recognition and Image Processing (PRIP)
Vienna University of Technology, Austria
{*christoph,ines,krw*}*@prip.tuwien.ac.at*

Abstract
In this paper, we briefly introduce the SCIS algorithm - a hierarchical image segmentation approach based on LBP pyramids - and evaluate its robustness to uniform, Gaussian, and Poisson distributed additive chromatic noise. Moreover, we study the influence of image properties such as the amount of details and SNR on the segmentation performance. Our evaluation shows that SCIS is robust to Gaussian and Poisson noise for our testing environment.

1. Introduction

Local binary patterns (LBPs) were originally introduced as a texture descriptor by Ojala et al. in 1994 [14]. Due to their computational simplicity and their robustness to varying lighting conditions LBPs have since become popular texture operators. In order to compute the LBP for a certain pixel, this pixel is compared to its subsampled neighbourhood. In case the value of a neighbouring pixel is larger than or equal to the value of the center pixel its bit is set to 1 otherwise to 0. The resulting bit pattern thus describes the neighbourhood relations. The bit pattern may be transformed to a decimal number by encoding each neighbourhood pixel using its position in a binary data item.
Image pyramids provide a multiscale representation of an image by applying smoothing and subsampling to this image repeatedly. Burt proposed in 1981 such an approach using a Gaussian like smoothing [1]. The well known Laplacian pyramid was later introduced by Burt and Adelson in [2]. For the Laplacian pyramid (except for the top level) the difference images of successive layers of a Gaussian pyramid are stored instead of the Gaussian smoothed images itself. A reconstruction of the original image is possible based on its Laplacian pyramid representation. Image pyramids are for example used when computing multi-scale image features as it is done by SIFT (scale invariant feature transform) [11] or for image compression (as described in [2]).
Both LBPs and image pyramids among other applications have been used individually in image segmentation algorithms:
Chen et al. [5] and Heikkilä et al. [8] for example use LBPs for segmentation purposes. These approaches however use LBP histograms, the spatial information of LBPs is therefore lost. Two visually completely different images may have the same LBP histogram - a major drawback of these approaches.
For hierarchical image segmentation a wide range of approaches has been published in the past: Kropatsch et al. present in [9] a hierarchical segmentation method based on minimum weight spanning trees of graph pyramids. A similar approach that allows user interaction during the segmentation process is presented by Gerstmayer et al. in [7]. A hierarchical image segmentation approach based on the feature detector MSER (maximally stable extremal regions) was proposed by Oh et al. in [13].
In this paper we discuss a recent image segmentation approach that combines LBPs and combinatorial pyramids - the structurally correct image segmentation algorithm (SCIS) introduced by Cerman [3]. Using this approach highly textured regions are merged late in the segmentation hierarchy. Thus,

preserving visual information that is important for human perception up to high levels of the pyramid. It is known that standard image pyramids such as Gaussian and Laplacian pyramids as well as hierarchical representations based on these concepts eliminate noise in the image due to the repeated smoothing operation [6]. However, since regions showing noise may also be consider as highly textured regions this may not be the case for SCIS. Therefore, we analyze the noise robustness of SCIS in this paper.

The rest of the paper is structured as follows: A short introduction to the SCIS algorithm is given in Section 2. Its robustness to noise is tested in experiments presented in Section 3. Results of these experiments are discussed in Section 4. Section 5. concludes the paper and gives an outlook to future work.

2. Structurally Correct Image Segmentation

The "structurally correct image segmentation" (SCIS) algorithm was first presented in [3]. Although, SCIS is based on LBPs it does not use histograms. This hierarchical segmentation approach constructs an irregular graph pyramid (sequence of reduced graphs), by iteratively identifying and removing redundant structural information, and merging regions with the lowest dissimilarity first.

The SCIS algorithm represents an image as a directed acyclic graph. Each vertex corresponds to a pixel, a superpixel or a region, and each edge corresponds to an adjacency relationship between two pixels, superpixels or regions. After merging neighboring vertices with equal grayscale-/color values, it is possible to assign each edge a direction, and thus describing the relationship between adjacent vertices as strict inequality relationships. As a result, this merging induces a strict partial order onto the vertices of the image graph. This ordering of the vertices is not a total ordering, because not all pairs of vertices are comparable by following monotonically increasing or decreasing paths. An edge is said to be "structurally redundant", if the removal of this edge does not break the reachability property of the graph. The SCIS algorithm identifies most of these redundant edges in a fast manner by means of a primal and dual topological LBP classification (see [4] for more detailed information) and removes them.

SCIS (see Algorithm 1) employs this idea, mentioned as *simplifying the structure* in algorithm 1 (line 5-8). Structurally redundant dual edges are determined and removed. Subsequently, regions with the lowest dissimilarity are merged. In the case of grayscale images, the absolute region intensity difference $d(x, y) = |g(x) - g(y)|$ is used, where x and y are two regions, and $g(x)$ is the

Algorithm 1 structurally correct image segmentation (SCIS)

input: 2D image
output: combinatorial pyramid

1: $k := 0$
2: initialize base level C of combinatorial pyramid
3: $C' :=$ remove dual saddles in C
4: $C_0 :=$ merge plateaus in C'
5: **repeat**
6: $\quad k := k + 1$
7: $\quad$ simplify structure in current level C_k
8: **until** $C_k = C_{k-1}$

intensity of x. For color images, the current implementation uses the CIEDE2000 color difference [15]. During the merging of regions, the algorithm computes the new value of the region as the mean value of all included pixels, and verifies, if this merging does not break the strict partial ordering of the previous graph.
In practice it is sufficient to remove redundant dual edges and to check that a newly computed value fits the surrounding LBP values. The remaining dual edges are then sorted according to their contrast. The dual edge with the lowest contrast is considered first and checked if it can be merged. Therefore, a new value for the merged dual vertices is computed (in our case this is the color mean) and if this value satisfies the binary relationships stored at the incident dual edges the edge is contracted. If not, the dual edge with the next lowest contrast is considered. This process is repeated until a suitable dual edge for merging is found. This way, by removing edges with the lowest contrast first, regions with low contrast are merged first.
Therefore, visual information that is important for humans is preserved even at high levels of reduction since highly textured regions are merged late in the hierarchy. This way, around 70 percent of regions can be merged in an image, with only a minimal loss of information important to humans. In many cases, merging up to around 94 percent is possible with visually acceptable results.

3. Experimental Setup

Depending on the technology for capturing a picture (analog or digital) and storing the picture (compressed or uncompressed) various types of noise are introduced to the resulting image. In this paper, the SCIS algorithm is evaluated regarding its robustness to common types of noise in digital images, such as quantization noise, sensor noise and shot noise.

3.1. Types of Noise

Quantization noise is introduced when the sensor of a digital camera maps the incoming light intensity to quantized levels of color values for each pixel. For the experiments, this noise type is modeled as uniform distributed chromatic additive noise with an amplitude of 50; the average SNR of the test images is $-9.03 \pm 0.34dB$. Figure 1a shows the normalized distribution of the quantization noise model.
Sensor noise can be caused by multiple environmental effects in a digital image sensor, such as bad lighting conditions, thermal conditions, and many more. For the experiments, this noise type is modeled as a Gaussian distributed chromatic additive noise with a σ of 5 and centered around 0; the average SNR of the test images is $6.20 \pm 0.34dB$. Figure 1b shows the normalized distribution of the sensor noise model.
Shot noise is introduced due to the fluctuations of the amount of photons that hit the sensor for a given exposure. For the experiments, this noise type is modeled as Poisson distributed chromatic additive noise with a λ of 50 centered around 0; the average SNR of the test images is $3.19 \pm 0.33dB$. Figure 1c shows the normalized distribution of the shot noise model.
Figure 2 shows these noise types applied to a sample image.

3.2. Image Data Set and Ground Truth

The SCIS algorithm is tested on 26 animal and landscape images of the Berkeley Image Segmentation data set [12] (see Figure 2a for a sample test image). This data set includes multiple ground truth segmentations per test image which have been segmented by humans. For the evaluation of the segmentation error for each test image, the first ground truth reference in alphabetic order is used (see Figure 2b for a sample ground truth image).

The segmentation error is evaluated on the reconstructed grayscale images of the LBP pyramid on a range from 0 to 5000 segments. Figure 3 shows the reconstructed images of the LBP pyramid for 200, 500, 1000 and 2000 segments as well as the magnitudes of the 2D Fourier transform. It is well visible that the frequencies are evenly distributed. A Fourier transform of a Laplacian pyramid shows circular structures due to the bandpass effect of this pyramid, for a Gaussian pyramid lowpass effects are visible in the frequency domain. Since these effects are not visible in the Fourier transforms of the LBP pyramid we conclude that the LBP pyramid does not have a bandpass nor a lowpass effect.

3.3. Validation Methodology

For estimating the empirical segmentation error against the ground truth images, the region-based segmentation measurement Global Consistency Error (GCE) [12] is used. It is a robust technique and independent of the number of segments in each image. The GCE is defined as:

$$GCE(S_1, S_2) = \frac{1}{n} min\Big(\sum_i E(S_1, S_2, p_i), \sum_i E(S_2, S_1, p_i)\Big) \tag{1}$$

To measure the same local refinement error E when changing the order of the reference image such that $E(S_1, S_2, p_i) = E(S_2, S_1, p_i)$, we take the minimum of both sums over all pixels in the GCE computation. In order to define E, we first denote the set difference of A and B as $A \setminus B$, and $|A|$ the cardinality of the set A. Let $R(S, p_i)$ be the set of pixels in the segmented image S that correspond to the region R containing pixels p_i, then the local refinement error E is defined as:

$$E(S_1, S_2, p_i) = \frac{|R(S_1, p_i) \setminus R(S_2, p_i)|}{|R(S_1, p_i)|} \tag{2}$$

4. Results

The GCE error is evaluated for all 26 test images for the range of 0 to 5000 segments, both for the reconstruction of the original images and of the noisy images. Figure 4 shows the original and the noisy images reconstructed with a different number of segments (compare with Figure 2b showing the ground truth).

As we can observe in Figure 4b, we expect the noise to introduce additional high frequencies to the original image and hence to result in smaller regions compared to the reconstruction of the original image (Figure 4a) for the same number of segments. For a bigger SNR, this effect should be less visible such as in Figure 4c and 4d.

Figure 5a shows the GCE evaluation of the reconstructed test images with an increasing number of segments. If one compares the GCE obtained from the original segmentation to the segmentation of the images with uniformly distributed noise (see Figure 5b), we observe that the GCE curves are

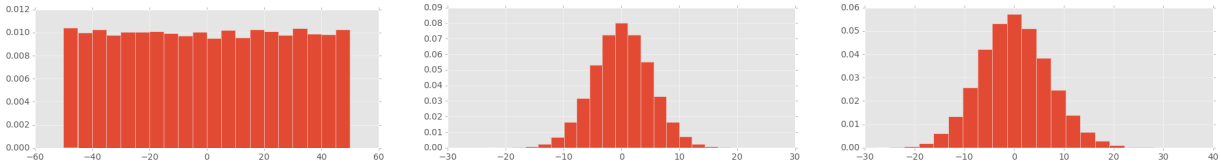

(a) Uniform noise (b) Gaussian noise (c) Poisson noise

Figure 1: Normalized noise distributions

(a) Original (105025.jpg)

(b) Ground truth

(c) Uniform noise

(d) Gaussian noise

(e) Poisson noise

Figure 2: Image with overlaying noise

(a) 200 segments

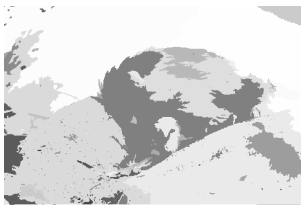

(b) 500 segments

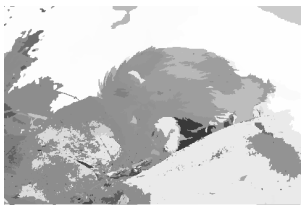

(c) 1000 segments

(d) 2000 segments

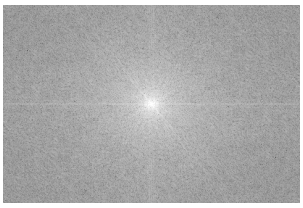

(e) 2D FFT of 200 segm.

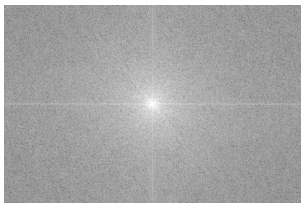

(f) 2D FFT of 500 segm.

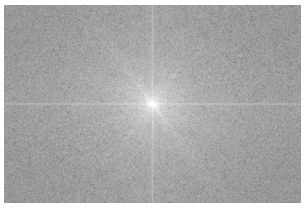

(g) 2D FFT of 1000 segm.

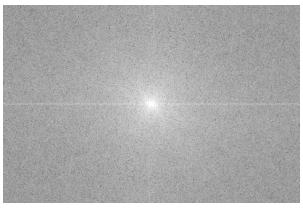

(h) 2D FFT of 2000 segm.

Figure 3: Reconstructions from the LBP pyramid (top) and their Fourier transforms (bottom).

shifted to the right (towards increasing number of segments). The shift is around 200 to 500 segments for images with a low SNR and between 500 and 1500 segments for images with a better SNR. For Gaussian (see Figure 5c) and Poisson (see Figure 5d) distributed noise the shifts are more concentrated between 200 and 1000 segments and the GCE curve rises steeper.

However, this is not exactly the behavior that we were expecting. A shift of the GCE curve to the right means that for the same number of segments the GCE of the noisy image is lower than for the original image. This effect can be better observed when looking at the difference of the GCE from the reconstruction of the test images and noisy images in Figure 6, in the range of 200 to 1500 segments. In this figure, a positive value corresponds with a lower GCE than in the original image whereas a negative value corresponds with a greater GCE.

For uniformly distributed noise (see Figure 6a), we can differentiate between 2 types of images in the range below 1500 segments: one group with a lower GCE than the original images and the other group with a greater GCE. These image groups correlate with the amount of details in an image as

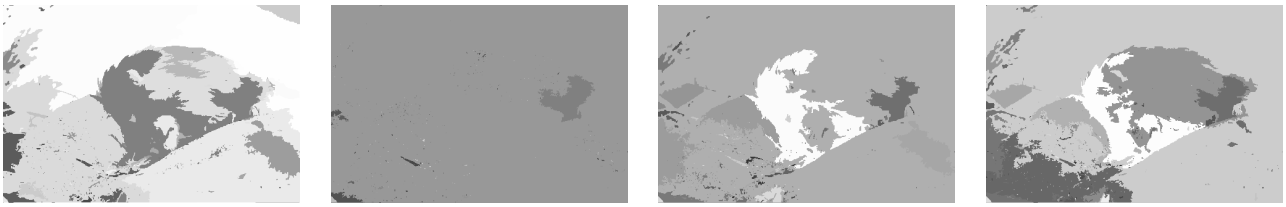

(a) Original 500 seg. (b) Uniform noise 500 seg. (c) Gaussian noise 500 seg. (d) Poisson noise 500 seg.

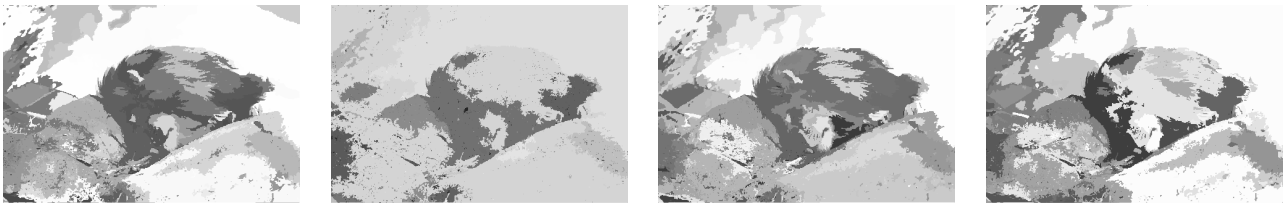

(e) Original 2000 seg. (f) Uniform noise 2000 seg. (g) Gaussian noise 2000 seg. (h) Poisson noise 2000 seg.

Figure 4: Reconstructed original and noisy images

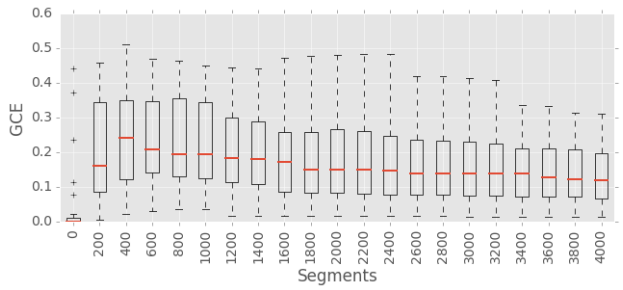

(a) Original images

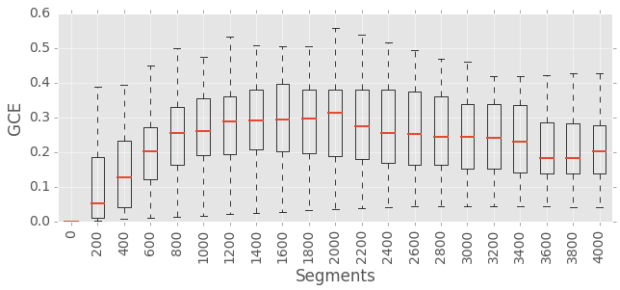

(b) Images with uniform noise

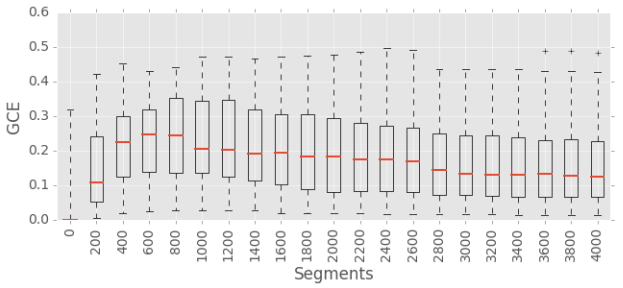

(c) Images with Gaussian noise

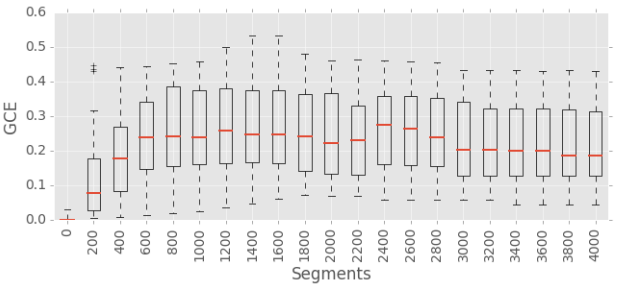

(d) Images with Poisson noise

Figure 5: GCE segmentation error of the test images and noisy images

well as the SNR: high amount of details (low SNR) and average amount of details (higher SNR). The latter group of images corresponds with the previously expected behavior.

For images with Gaussian distributed noise (see Figure 6b), we conclude that the GCE is almost the same as for the original images with a few outliers at maximal difference of 0.2. The Poisson distributed noise (see Figure 6c) has a similar behavior to uniformly distributed noise but less outliers.

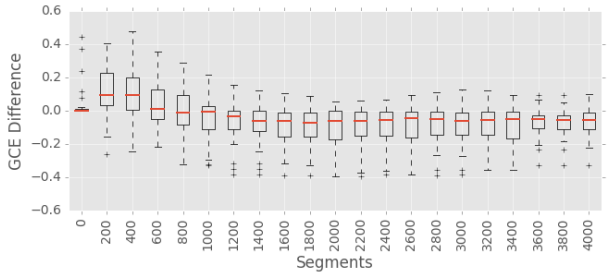

(a) Images with uniform noise

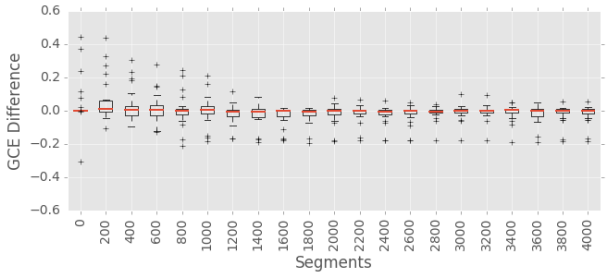

(b) Images with Gaussian noise

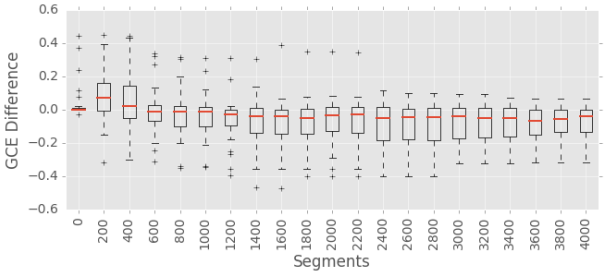

(c) Images with Poisson noise

Figure 6: Difference of the GCE segmentation error of original images and noisy images

5. Conclusion

The SCIS algorithm shows a maximal decrease of 0.2 for outliers in the GCE for images with Gaussian distributed noise for reconstructions using more than 200 segments (see Figure 6b). The GCE stays the same also for increasing σ and sometimes gets even lower for reconstructions using less than 1000 segments. Hence, it can be said that the SCIS is robust to Gaussian noise under the constraints of the testing environment.

For reconstructions using less than 1000 segments, the SCIS algorithm is very sensitive to uniform noise leading to both better and worst segmentation result strongly depending on the SNR and the amount of details in the image (see Figures 5b and 6a). Also for reconstructions using more than 1000 segments, the mean difference to the original GCE is around 0.075 with many outliers around 0.4. However, it should be noted that the tested noise amplitude was slightly higher compared to quantization noise in common digital sensors.

For Poisson distributed noise, the mean difference to original GCE values is less than 0.05 for reconstructions above 1000 segments with only a few outliers up to 0.5. For less segments, the behavior is similar to uniform distributed noise. Hence, we conclude that the SCIS algorithm is also robust to Poisson noise under the constraints of the testing environment.

We have shown that SCIS algorithm achieves good segmentation results for images with chromatic additive Gaussian and Poisson distributed noise and is sensitive to uniformly distributed noise. The experiments could be extended to also evaluate monochromatic noise and other relevant noise types e.g. Salt-and-pepper noise.

Acknowledgments

We thank Martin Cerman for assistance with the SCIS algorithm and helpful comments on the experiments and interpretation of the results.

References

[1] P. J. Burt. *Fast filter transform for image processing.* Computer graphics and image processing vol.16.1 pp. 20–51 (1981).

[2] P. J. Burt, E. H. Adelson. *The Laplacian pyramid as a compact image code.* IEEE Transactions on Communications. vol.31.4 pp. 532–540 (1983).

[3] M. Cerman: *Structurally Correct Image Segmentation using Local Binary Patterns and the Combinatorial Pyramid*. Technical Report 133[1], Vienna University of Technology, Pattern Recognition and Image Processing (PRIP) Group. (2015)

[4] M. Cerman; R. Gonzalez-Diaz; W. G. Kropatsch: *LBP and Irregular Graph Pyramids.* In the Proceedings of CAIP 2015, Part II, pp.687-699 (2015).

[5] J. Chen, S. Shan, C. He, G. Zhao, M. Pietikäinen, X. Chen, W. Gao. *WLD: A robust local image descriptor*. IEEE TPAMI, vol. 32(9), pp. 1705–1720 (2010)

[6] S. Contassot-Vivier, G. L. Bosco, N. C. Dao. *Multiresolution approach for image processing.* Erasmus ICP-A-2007 (1996).

[7] M. Gerstmayer, Y. Haxhimusa, W. G. Kropatsch. *Hierarchical interactive image segmentation using irregular pyramids.* Graph-Based Representations in Pattern Recognition. Springer Berlin Heidelberg, pp.245–254 (2011).

[8] M. Heikkilä, M. Pietikäinen: *A texture-based method for modeling the background and detecting moving objects*. IEEE TPAMI, vol. 28(4), pp. 657–662 (2006).

[9] W. G. Kropatsch,Y. Haxhimusa, A. Ion *Multiresolution image segmentations in graph pyramids.* Applied Graph Theory in Computer Vision and Pattern Recognition, Springer Berlin Heidelberg, pp. 3–41 (2007).

[10] LBP'2014 Workshop on Computer Vision With Local Binary Pattern Variants [2]

[11] D. G. Lowe. *Distinctive image features from scale-invariant keypoints.* International journal of computer vision vol.60.2 pp.91–110 (2004).

[12] D. Martin; C. Fowlkes; C. Tal; J. Malik: *A database of human segmented natural images and its application to evaluating segmentation algorithms and measuring ecological statistics.* In the Proceedings of ICCV 2001, pp.416-423 (2001).

[13] I.S. Oh, J. Lee, A. Majumder. *Multi-scale image segmentation using MSER.* In the Proceedings of CAIP 2013, Part II, pp. 201–208 (2013).

[14] T. Ojala, M. Pietikainen, D. Harwood. *Performance evaluation of texture measures with classification based on Kullback discrimination of distributions.* Proceedings of ICPR 1994, pp. vol.1 582-585 (1994).

[15] G. Sharma, W. Wu, E. N. Dalal. *The CIEDE2000 Color-Dierence Formula: Implementation Notes*, Supplementary Test Data, and Mathematical Observations. Color Research and Rpplication, vol.30.1 pp.21–30 (2005).

[1] ftp://ftp.prip.tuwien.ac.at/pub/publications/trs/tr133.pdf

[2] https://sites.google.com/site/lbp2014ws/